# Supplementary Material for: Transition Moments Beyond the Electric-Dipole Approximation: Visualization and Basis Set Requirements

Martin van Horn,[*,†] Nanna Holmgaard List,[*,‡] and Trond Saue[*,†]

†*Laboratoire de Chimie et Physique Quantique, UMR 5626 CNRS — Université Toulouse III-Paul Sabatier, 118 route de Narbonne, F-31062 Toulouse, France.*

‡*Department of Chemistry, School of Engineering Sciences in Chemistry, Biotechnology and Health (CBH), KTH Royal Institute of Technology, SE-10044 Stockholm, Sweden.*

E-mail: mvanhorn@irsamc.ups-tlse.fr; nalist@kth.se; trond.saue@irsamc.ups-tlse.fr

# Contents

# S1 Transition moments from response theory

## S1.1 Quasienergy formalism

In exact-state response theory transition moments and excitation energies can be extracted from the linear response function[1]

$$\langle\langle \hat{A}; \hat{B} \rangle\rangle_{\omega} = -\frac{1}{\hbar} \sum_{n} \left\{ \frac{\langle 0|\hat{A}|n\rangle\langle n|\hat{B}|0\rangle}{(\omega_{n0} - \omega)} + \frac{\langle 0|\hat{B}|n\rangle\langle n|\hat{A}|0\rangle}{(\omega_{n0} + \omega)} \right\}. \tag{S1}$$

The purpose of this section is to investigate the definition of transition moments in approximate-state response theory.

We shall work within the quasienergy formalism[2,3] where the perturbed wave function is written as

$$|\overline{0}\rangle = \exp\left[-\frac{i}{\hbar} F(t)\right] |\tilde{0}\rangle.$$

Inserted into the time-dependent wave function, one obtains

$$\left(\hat{H} - i\hbar\partial_t\right) |\tilde{0}\rangle = \mathcal{Q}(t) |\tilde{0}\rangle,$$

where appears the time-dependent quasienergy

$$\mathcal{Q}(t) = \dot{F}(t) = \langle\tilde{0}| \left(\hat{H} - i\hbar\partial_t\right) |\tilde{0}\rangle.$$

In order to connect expectation values and derivatives of the quasienergy, in the static case provided by the Hellmann–Feynman theorem, we restrict the Hamiltonian to the time-periodic case

$$\hat{H}(t + T) = \hat{H}(t),$$

and work with the time-averaged quasienergy

$$Q = \{\mathcal{Q}(t)\}_T; \quad \{f(t)\}_T = \frac{1}{T}\int_{-T/2}^{+T/2} f(t)\, dt.$$

Partitioning the Hamiltonian $\hat{H}$ into an unperturbed, time-independent part $\hat{H}_0$ and a perturbation operator

$$\hat{V}(t) = \int_{-\infty}^{+\infty} \hat{V}(\omega)\, e^{-i\omega t} dt,$$

we find that hermiticity implies

$$\hat{V}^\dagger(t) = \hat{V}(t) \quad \Rightarrow \quad \hat{V}^\dagger(\omega) = \hat{V}(-\omega),$$

whereas time-periodicity implies

$$\hat{V}(t) = \hat{V}(t+T) \quad \Rightarrow \quad \omega = n\omega_T; \quad \omega_T = \frac{2\pi}{T}, \quad n \in \mathbb{N}.$$

We shall therefore write the perturbation operator as

$$\hat{V}(t) = \sum_{k=-N}^{N} \exp[-i\omega_k t] \sum_X \varepsilon_X(\omega_k)\, \hat{h}_X$$

where all frequencies are integer multiplies of the fundamental frequency $\omega_T$ and where $\hat{h}_X$ and $\varepsilon_X(\omega_k)$ are perturbation operators and associated strengths, respectively.

In the following we make use of variational perturbation theory, where the time-averaged quasienergy is assumed to be optimized at *all* field strengths, thus making the variational parameters *functions* of the perturbation strengths. We shall consider response theory at the CI and HF levels.

## S1.2 CI response theory

We write the (perturbed) phase-isolated wave function as

$$|\tilde{0}\,(t)\rangle = \exp\left[-\hat{S}\,(t)\right]|0\rangle; \quad \hat{S}\,(t) = \sum_{mn} S_{mn}\,(t)\,|m\rangle\langle n|, \quad S^*_{mn} = -S_{nm}$$

where the state-rotation operator $\hat{S}$ is anti-Hermitian to assure that the exponential parametrization is unitary. $\{|n\rangle\}$ refers to an orthonormal $N$-electron basis, where the reference $|0\rangle$ is a solution of $\hat{H}_0$ in a variational sense.

The quasi-energy now reads

$$Q = \left\{\langle 0|\exp\left[\hat{S}\,(t)\right]\left(\hat{H} - i\hbar\partial_t\right)\exp\left[-\hat{S}\,(t)\right]|0\rangle\right\}_T.$$

A Baker–Campbell–Hausdorff (BCH) expansion

$$\begin{aligned} Q &= \left\{\langle 0|\left(\hat{H} - i\hbar\partial_t\right)|0\rangle\right\}_T \\ &+ \left\{\langle 0|\left[\hat{S}\,(t)\,,\left(\hat{H} - i\hbar\partial_t\right)\right]|0\rangle\right\}_T \\ &+ \left\{\frac{1}{2}\langle 0|\left[\hat{S}\,(t)\,,\left[\hat{S}\,(t)\,,\left(\hat{H} - i\hbar\partial_t\right)\right]\right]|0\rangle\right\}_T + \ldots \end{aligned}$$

provides a convenient expansion in orders of the state-rotation amplitudes $S_{mn}\,(t)$. For the first-order term we obtain

$$Q_1 = \left\{\langle 0|\left[\hat{S}\,(t)\,,\left(\hat{H} - i\hbar\partial_t\right)\right]|0\rangle\right\}_T = \left\{\sum_n \left(S_{0n}\,(t)\,\langle n|\hat{H}|0\rangle - S_{n0}\,(t)\,\langle 0|\hat{H}|n\rangle\right) + i\hbar\dot{S}_{00}\,(t)\right\}_T. \tag{S2}$$

Inspection of the first-order term allows the elimination of redundant variational parameters. From Eq. (S2) it is clear that only amplitudes involving the reference determinant contributes. However, it is clear that the time-dependent set $\{S_{mn}\,(t)\}$ can not serve as variational parameters with respect to the *time-independent* quasienergy. We shall therefore

instead work with the Fourier components $\{S_{mn}(\omega)\}$. It can be shown that the amplitudes inherits the periodicity of the Hamiltonian,[3,4] so that we may write

$$S_{mn}(t) = \sum_{k=-N}^{N} \exp[-i\omega_k t] S_{mn}(\omega_k).$$

This also implies that the final term of (S2) vanishes upon time averaging. Furthermore, contributions from $n = 0$ vanishes in the first term, leading to the non-redundant parametrization

$$\hat{S}(t) = \sum_{k=-N}^{N} \exp[-i\omega_k t] \sum_{n}{}' \left(S_{n0}(\omega_k)|n\rangle\langle 0| - S^*_{n0}(-\omega_k)|0\rangle\langle n|\right),$$

where the prime on the summation symbol indicates that the contribution $n = 0$ is omitted. Notice how excitations $|n\rangle\langle 0|$ are now associated with parameters $S_{n0}(\omega_k)$ and de-excitations $|0\rangle\langle n|$ with parameters $S^*_{n0}(-\omega_k)$, the anti-resonant partners.

We shall assume that the quasienergy is fully optimized at all field strenghts, that is

$$\left[\frac{\partial Q}{\partial S_{n0}(\omega_k)}\right]_{\boldsymbol{\varepsilon}} = 0 = \left[\frac{\partial Q}{\partial S^*_{n0}(-\omega_k)}\right]_{\boldsymbol{\varepsilon}}, \quad \forall S_{n0}(\omega_k), \tag{S3}$$

where the vector $\boldsymbol{\varepsilon}$ collects the perturbation strengths. We shall define elements of the gradient as the above derivatives, taken at *zero* field strength. We then obtain

$$\begin{array}{rcccl} \left[\frac{\partial Q}{\partial S^*_{n0}(-\omega_k)}\right]_{\boldsymbol{\varepsilon}=\mathbf{0}} & = & \left[\frac{\partial}{\partial S^*_{n0}(-\omega_k)}\left\{\langle 0|\left[\hat{S}(t), \left(\hat{H} - i\hbar\partial_t\right)\right]|0\rangle\right\}_T\right]_{\boldsymbol{\varepsilon}=\mathbf{0}} & = & -\langle n|\hat{H}_0|0\rangle\delta(\omega_k) \\ \left[\frac{\partial Q}{\partial S_{n0}(\omega_k)}\right]_{\boldsymbol{\varepsilon}=\mathbf{0}} & = & \left[\frac{\partial}{\partial S_{n0}(\omega_k)}\left\{\langle 0|\left[\hat{S}(t), \left(\hat{H} - i\hbar\partial_t\right)\right]|0\rangle\right\}_T\right]_{\boldsymbol{\varepsilon}=\mathbf{0}} & = & -\langle 0|\hat{H}_0|n\rangle\delta(\omega_k) \end{array}. \tag{S4}$$

We see that these elements are zero when the reference does not couple through $\hat{H}_0$ to the orthogonal complement $\{|n\rangle\}_{n\neq 0}$.

From the variational condition Eq. (S3), the first perturbation derivative, at any field

strength, therefore reads

$$\frac{dQ}{d\varepsilon_A(\omega_a)} = \frac{\partial Q}{\partial \varepsilon_A(\omega_a)} + \sum_{\ell m} \frac{\partial Q}{\partial S_{m0}(\omega_\ell)} \frac{\partial S_{m0}(\omega_\ell)}{\partial \varepsilon_A(\omega_a)} + \sum_{\ell m} \frac{\partial Q}{\partial S^*_{m0}(-\omega_\ell)} \frac{\partial S^*_{m0}(-\omega_\ell)}{\partial \varepsilon_A(\omega_a)} = \frac{\partial Q}{\partial \varepsilon_A(\omega_a)}.$$

We are interested in the first perturbation derivative at zero perturbation at which the variational parameters are zero. We may therefore develop

$$\left[\frac{dQ}{d\varepsilon_A(\omega_a)}\right]_{\boldsymbol{\varepsilon}=\mathbf{0}} = \left[\frac{\partial Q}{\partial \varepsilon_A(\omega_a)}\right]_{\boldsymbol{\varepsilon}=\mathbf{0}} = \left\{\langle 0|\hat{h}_A|0\rangle \exp\left[-i\omega_a t\right]\right\}_T = \langle 0|\hat{h}_A|0\rangle \delta(\omega_a),$$

and we see that we indeed recover the Hellmann–Feynman theorem.

Continuing to the second perturbation derivative at zero perturbation, we get

$$\begin{aligned}\left[\frac{d^2Q}{d\varepsilon_A(\omega_a)\, d\varepsilon_B(\omega_b)}\right]_{\boldsymbol{\varepsilon}=\mathbf{0}} &= \left[\frac{\partial^2 Q}{\partial \varepsilon_A(\omega_a)\, \partial \varepsilon_B(\omega_b)} + \sum_{\ell m} \frac{\partial^2 Q}{\partial \varepsilon_A(\omega_a)\, \partial S_{m0}(\omega_\ell)} \frac{\partial S_{m0}(\omega_\ell)}{\partial \varepsilon_B(\omega_b)}\right]_{\boldsymbol{\varepsilon}=\mathbf{0}} \\ &+ \left[\sum_{\ell m} \frac{\partial^2 Q}{\partial \varepsilon_A(\omega_a)\, \partial S^*_{m0}(-\omega_\ell)} \frac{\partial S^*_{m0}(-\omega_\ell)}{\partial \varepsilon_B(\omega_b)}\right]_{\boldsymbol{\varepsilon}=\mathbf{0}} \end{aligned} \tag{S5}$$

The first term vanishes to the extent that the wave function has no explicit perturbation-dependence and the perturbation operator is linear in perturbation strengths (in the non-relativistic domain this is not generally true). It will be ignored in the following.

We now need first-order perturbed amplitudes. They can be obtained from the variational conditions Eq. (S3). Specifically, we use

$$\begin{aligned} 0 &= \left[\frac{d}{d\varepsilon_B(\omega_b)} \frac{\partial Q}{\partial S_{n0}(\omega_k)}\right]_{\boldsymbol{\varepsilon}=\mathbf{0}} = \left[\frac{\partial^2 Q}{\partial \varepsilon_B(\omega_b)\, \partial S_{n0}(\omega_k)}\right]_{\boldsymbol{\varepsilon}=\mathbf{0}} \\ &+ \left[\sum_{\ell m} \frac{\partial^2 Q}{\partial S_{n0}(\omega_k)\, \partial S_{m0}(\omega_\ell)} \frac{\partial S_{m0}(\omega_\ell)}{\partial \varepsilon_B(\omega_b)} + \sum_{\ell m} \frac{\partial^2 Q}{\partial S_{n0}(\omega_k)\, \partial S^*_{m0}(-\omega_\ell)} \frac{\partial S^*_{m0}(-\omega_\ell)}{\partial \varepsilon_B(\omega_b)}\right]_{\boldsymbol{\varepsilon}=\mathbf{0}} \\ 0 &= \left[\frac{d}{d\varepsilon_B(\omega_b)} \frac{\partial Q}{\partial S^*_{n0}(-\omega_k)}\right]_{\boldsymbol{\varepsilon}=\mathbf{0}} = \left[\frac{\partial^2 Q}{\partial \varepsilon_B(\omega_b)\, \partial S^*_{n0}(-\omega_k)}\right]_{\boldsymbol{\varepsilon}=\mathbf{0}} \\ &+ \left[\sum_{\ell m} \frac{\partial^2 Q}{\partial S^*_{n0}(-\omega_k)\, \partial S_{m0}(\omega_\ell)} \frac{\partial S_{m0}(\omega_\ell)}{\partial \varepsilon_B(\omega_b)} + \sum_{\ell n} \frac{\partial^2 Q}{\partial S^*_{n0}(-\omega_k)\, \partial S^*_{m0}(-\omega_\ell)} \frac{\partial S^*_{m0}(-\omega_\ell)}{\partial \varepsilon_B(\omega_b)}\right]_{\boldsymbol{\varepsilon}=\mathbf{0}} \end{aligned}$$

Let us now look at individual terms, first the property gradient. We find

$$\begin{aligned}
\left[\frac{\partial^2 Q}{\partial\varepsilon_B(\omega_b)\,\partial S_{n0}(\omega_k)}\right]_{\boldsymbol{\varepsilon}=\mathbf{0}} &= \left[\frac{\partial^2}{\partial\varepsilon_B(\omega_b)\,\partial S_{n0}(\omega_k)}\left\{\langle 0|\left[\hat{S}(t),\left(\hat{H}-i\hbar\partial_t\right)\right]|0\rangle\right\}_T\right]_{\boldsymbol{\varepsilon}=\mathbf{0}} \\
&= -\langle 0|\hat{h}_B|n\rangle\delta(\omega_k+\omega_b) \\
\left[\frac{\partial^2 Q}{\partial\varepsilon_B(\omega_b)\,\partial S^*_{n0}(-\omega_k)}\right]_{\boldsymbol{\varepsilon}=\mathbf{0}} &= -\langle n|\hat{h}_B|0\rangle\delta(\omega_k+\omega_b)
\end{aligned}$$

We next look at elements of the second-derivative matrix at zero perturbation strength. This corresponds to taking corresponding derivatives of the second-order quasienergy

$$Q_2 = \left\{\frac{1}{2}\langle 0|\left[\hat{S}(t),\left[\hat{S}(t),\hat{H}\right]\right]|0\rangle + \frac{1}{2}i\hbar\langle 0|\left[\hat{S}(t),\dot{\hat{S}}(t)\right]|0\rangle\right\}_T.$$

We obtain

$$\begin{aligned}
\left[\frac{\partial^2 Q}{\partial S^*_{n0}(-\omega_k)\,\partial S_{m0}(\omega_\ell)}\right]_{\boldsymbol{\varepsilon}=\mathbf{0}} &= \left(\langle n|\hat{H}_0|m\rangle - \delta_{mn}\langle 0|\hat{H}_0|0\rangle + \hbar\omega_k\delta_{mn}\right)\delta(\omega_k+\omega_\ell) \\
\left[\frac{\partial^2 Q}{\partial S^*_{n0}(-\omega_k)\,\partial S^*_{m0}(-\omega_\ell)}\right]_{\boldsymbol{\varepsilon}=\mathbf{0}} &= 0 \\
\left[\frac{\partial^2 Q}{\partial S_{n0}(\omega_k)\,\partial S_{m0}(\omega_\ell)}\right]_{\boldsymbol{\varepsilon}=\mathbf{0}} &= 0 \\
\left[\frac{\partial^2 Q}{\partial S_{n0}(\omega_k)\,\partial S^*_{m0}(-\omega_\ell)}\right]_{\boldsymbol{\varepsilon}=\mathbf{0}} &= \left(\langle m|\hat{H}_0|n\rangle - \delta_{mn}\langle 0|\hat{H}_0|0\rangle - \hbar\omega_k\delta_{mn}\right)\delta(\omega_\ell+\omega_k)
\end{aligned}$$

With these quantities at hand, we can return to the response equations

$$\begin{aligned}
\sum_m\left(\langle n|\hat{H}_0|m\rangle - \delta_{mn}\langle 0|\hat{H}_0|0\rangle - \delta_{mn}\hbar\omega_k\right)\left[\frac{\partial S_{m0}(-\omega_k)}{\partial\varepsilon_B(\omega_b)}\right]_{\boldsymbol{\varepsilon}=\mathbf{0}} &= \langle n|\hat{h}_B|0\rangle\delta(\omega_k+\omega_b) \\
\sum_m\left(\langle m|\hat{H}_0|n\rangle - \delta_{mn}\langle 0|\hat{H}_0|0\rangle + \delta_{mn}\hbar\omega_k\right)\left[\frac{\partial S^*_{m0}(\omega_k)}{\partial\varepsilon_B(\omega_b)}\right]_{\boldsymbol{\varepsilon}=\mathbf{0}} &= \langle 0|\hat{h}_B|n\rangle\delta(\omega_k+\omega_b)
\end{aligned} \tag{S6}$$

At this point we can note that the right-hand sides vanish unless $\omega_k = -\omega_b$.

The first-order response equations may be written as

$$\left(E_0^{[2]} - \hbar\omega_b S^{[2]}\right)\mathbf{X}_B(\omega_b) = -\mathbf{E}_B^{[1]} \tag{S7}$$

where appears the solution vector $\mathbf{X}_B(\omega_b)$ and the property gradient $\mathbf{E}_B^{[1]}$, and where the electronic Hessian $E_0^{[2]}$ and the generalized metric $S^{[2]}$ are Hermitian matrices. Their structures are

$$E_0^{[2]} = \begin{bmatrix} A & B \\ B^* & A^* \end{bmatrix}; \quad S^{[2]} = \begin{bmatrix} \Sigma & \Delta \\ \Delta^* & -\Sigma^* \end{bmatrix}; \quad \boldsymbol{X}_B(\omega_b) = \begin{bmatrix} \boldsymbol{Z} \\ \boldsymbol{Y}^* \end{bmatrix}; \quad \boldsymbol{E}_B^{[1]} = \begin{bmatrix} \boldsymbol{g}_B \\ \boldsymbol{g}_B^* \end{bmatrix}. \tag{S8}$$

In CI response theory we have

$$\begin{aligned} A_{nm} &= \langle n|\hat{H}_0|m\rangle - \delta_{nm}\langle 0|\hat{H}_0|0\rangle \quad ; \quad \Sigma_{nm} = \delta_{nm} \quad ; \quad Z_m = \left[\tfrac{\partial S_{m0}(\omega_b)}{\partial \varepsilon_B(\omega_b)}\right]_{\boldsymbol{\varepsilon}=\mathbf{0}} \\ B_{nm} &= 0 \qquad\qquad\qquad\qquad ; \quad \Delta_{nm} = 0 \quad ; \quad Y_m^* = \left[\tfrac{\partial S_{m0}^*(-\omega_b)}{\partial \varepsilon_B(\omega_b)}\right]_{\boldsymbol{\varepsilon}=\mathbf{0}} \\ g_{B,m} &= -\langle m|\hat{h}_B|0\rangle \end{aligned}$$

Important to note is that in CI response theory we have *identically* $B = \Delta = 0$. In this notation the linear response function can be expressed as

$$\left[\frac{d^2Q}{d\varepsilon_A(\omega_a)\, d\varepsilon_B(\omega_b)}\right]_{\boldsymbol{\varepsilon}=\mathbf{0}} \delta(\omega_a + \omega_b) = \boldsymbol{E}_A^{[1]\dagger} \boldsymbol{X}_B(\omega_b) = -\boldsymbol{E}_A^{[1]\dagger} \left(E_0^{[2]} - \hbar\omega_b S^{[2]}\right)^{-1} \boldsymbol{E}_B^{[1]}. \tag{S9}$$

In the *special* case where the $N$-particle basis are eigenfunctions of $\hat{H}_0$, we can immediately solve the for the first-order amplitudes to give

$$\begin{aligned} \left[\frac{\partial S_{m0}(-\omega_k)}{\partial \varepsilon_B(\omega_b)}\right]_{\boldsymbol{\varepsilon}=\mathbf{0}} &= \frac{\langle m|\hat{h}_B|0\rangle}{(E_m - E_0 + \hbar\omega_k)} \delta(\omega_k + \omega_b) \\ \left[\frac{\partial S_{m0}^*(\omega_k)}{\partial \varepsilon_B(\omega_b)}\right]_{\boldsymbol{\varepsilon}=\mathbf{0}} &= \frac{\langle 0|\hat{h}_B|m\rangle}{(E_m - E_0 - \hbar\omega_k)} \delta(\omega_k + \omega_b) \end{aligned}$$

Returning to the linear response function we get

$$\left[\frac{d^2Q}{d\varepsilon_A(\omega_a)\, d\varepsilon_B(\omega_b)}\right]_{\boldsymbol{\varepsilon}=\mathbf{0}} \delta(\omega_a + \omega_b) = -\left\{\sum_m \frac{\langle 0|\hat{h}_A|m\rangle\langle m|\hat{h}_B|0\rangle}{(E_m - E_0 - \hbar\omega_b)} + \frac{\langle 0|\hat{h}_B|m\rangle\langle m|\hat{h}_A|0\rangle}{(E_m - E_0 + \hbar\omega_b)}\right\}$$

This expression corresponds to Eq. (S1).

## S1.3 HF response theory

We write the (perturbed) phase-isolated wave function as

$$|\tilde{\Phi}_0(t)\rangle = \exp\left[-\hat{\kappa}(t)\right]|\Phi_0\rangle; \quad \hat{\kappa}(t) = \sum_{pq} \kappa_{pq}(t)\,\hat{a}_p^\dagger \hat{a}_q, \quad \kappa_{qp}^* = -\kappa_{pq}$$

where the orbital-rotation operator $\hat{\kappa}$ is anti-Hermitian, again to assure that the exponential parametrization is unitary. Indices $p, q, r, s, t$ refer to some orthonormal set of reference orbitals $\{\varphi_p\}$, whereas the reference $|\Phi_0\rangle$ is the HF solution associated with $\hat{H}_0$. In the following we use indices $i, j, k, l$ and $a, b, c, d$ to distinguish occupied and virtual orbitals. The overall Hamiltonian is expressed in second-quantization as

$$\hat{H} = \sum_{pq} h_{pq}\hat{a}_p^\dagger \hat{a}_q + \frac{1}{4}\sum_{pqrs} \mathcal{L}_{pq,rs}\hat{a}_p^\dagger \hat{a}_r^\dagger \hat{a}_s \hat{a}_q; \quad \mathcal{L}_{pq,rs} = (\varphi_p\varphi_q|g|\varphi_r\varphi_s) - (\varphi_p\varphi_s|g|\varphi_r\varphi_q),$$

where matrix elements of the one-electron part are written

$$h_{pq} = h_{0;pq} + \sum_{k=-N}^{N} \exp\left[-i\omega_k t\right] \sum_X \varepsilon_X(\omega_k)\, h_{X;pq}$$

An important observation is to note that we may write

$$\left[\hat{\kappa}(t), \hat{H}\right] = \hat{H}^{\{1\}} = \sum_{pq} h_{pq}^{\{1\}}\hat{a}_p^\dagger \hat{a}_q + \frac{1}{4}\sum_{pqrs} \mathcal{L}_{pq,rs}^{\{1\}}\hat{a}_p^\dagger \hat{a}_r^\dagger \hat{a}_s \hat{a}_q, \tag{S10}$$

where appears *one-index transformed* quantities

$$\begin{aligned} h_{pq}^{\{1\}} &= \sum_t \left(\kappa_{pt}h_{tq} - h_{pt}\kappa_{tq}\right) \\ \mathcal{L}_{pq,rs}^{\{1\}} &= \sum_t \left(\kappa_{pt}\mathcal{L}_{tq,rs} - \mathcal{L}_{pt,rs}\kappa_{tq} + \kappa_{rt}\mathcal{L}_{pq,ts} - \mathcal{L}_{pq,rt}\kappa_{ts}\right) \end{aligned} \tag{S11}$$

We note that the one-index transformation of the anti-symmetrized two-electron integrals is

carried out separately for each electron. For the first-order term we thereby obtain

$$Q_1 = \left\{ \langle \Phi_0 | \left[ \hat{\kappa}\left(t\right), \left( \hat{H} - i\hbar\partial_t \right) \right] | \Phi_0 \rangle \right\}_T = \left\{ \sum_i h_{ii}^{\{1\}} + \frac{1}{2} \sum_{ij} \mathcal{L}_{ii,jj}^{\{1\}} + i\hbar \sum_i \dot{\kappa}_{ii}\left(t\right) \right\}_T \quad \text{(S12)}$$

Proceeding as in the CI-problem above, we find that the non-redundant parametrization is given by

$$\hat{\kappa}\left(t\right) = \sum_{k=-N}^{N} \exp\left[-i\omega_k t\right] \sum_{ai} \left( \kappa_{ai}\left(\omega_k\right) \hat{a}_a^\dagger \hat{a}_i - \kappa_{ai}^*\left(-\omega_k\right) \hat{a}_i^\dagger \hat{a}_a \right).$$

Again excitations $a^\dagger i$ are associated with parameters $\kappa_{ai}\left(\omega_k\right)$ and de-excitations $i^\dagger a$ with the anti-resonant partners $\kappa_{ai}^*\left(-\omega_k\right)$.

In line with the tenets of variational perturbation theory, we assume that the HF determinant is optimized at all perturbation field strengths. For later use, we note that at zero field the variational condition, valid for our reference, reads

$$\begin{array}{rcccccc} \left[\frac{\partial Q}{\partial \kappa_{ai}^*(-\omega_k)}\right]_{\boldsymbol{\varepsilon}=\mathbf{0}} & = & -\langle \Phi_i^a | \hat{H}_0 | \Phi_0 \rangle & = & -F_{ai} & = & 0 \\ \left[\frac{\partial Q}{\partial \kappa_{ai}(\omega_k)}\right]_{\boldsymbol{\varepsilon}=\mathbf{0}} & = & -\langle \Phi_0 | \hat{H}_0 | \Phi_i^a \rangle & = & -F_{ia} & = & 0, \end{array} \quad \text{(S13)}$$

where we recognize Brillouin's theorem, which translates into the occupied–virtual blocks of the Fock matrix being zero.

The first-order response equations can be cast in the form of Eq. (S7). Elements of the electronic Hessian $E_0^{[2]}$ are

$$\begin{array}{rclcrcl} A_{ai,bj} & = & \langle \Phi_0 | \left[ -\hat{a}_i^\dagger \hat{a}_a, \left[ \hat{a}_b^\dagger \hat{a}_j, \hat{H}_0 \right] \right] \Phi_0 \rangle & \qquad & B_{ai,bj} & = & \langle \Phi_0 | \left[ \hat{a}_i^\dagger \hat{a}_a, \left[ \hat{a}_j^\dagger \hat{a}_b, \hat{H}_0 \right] \right] \Phi_0 \rangle \\ & = & \langle \Phi_i^a | \hat{H}_0 | \Phi_j^b \rangle - \delta_{ab}\delta_{ij} \langle \Phi_0 | \hat{H}_0 | \Phi_0 \rangle & & & = & \langle \Phi_{ij}^{ab} | \hat{H}_0 | \Phi_0 \rangle \\ & = & \delta_{ij} F_{ab} - \delta_{ab} F_{ji} - \mathcal{L}_{ab,ji} & & & = & \mathcal{L}_{ai,bj}, \end{array} \quad \text{(S14)}$$

whereas elements of the general metric $S^{[2]}$ are

$$\begin{aligned} \Sigma_{ai,bj} &= \langle\Phi_0|\left[-\hat{a}_i^\dagger\hat{a}_a, \hat{a}_b^\dagger\hat{a}_j\right]\Phi_0\rangle \qquad \Delta_{ai,bj} = \langle\Phi_0|\left[\hat{a}_i^\dagger\hat{a}_a, \hat{a}_j^\dagger\hat{a}_b\right]\Phi_0\rangle \\ &= \delta_{ab}\delta_{ij} \qquad\qquad\qquad\qquad = 0. \end{aligned} \tag{S15}$$

Elements of the property gradient $E_B^{[1]}$ are given by

$$g_{B;bj} = -\langle\Phi_j^b|\hat{h}_B|\Phi_0\rangle = -h_{B;bj}. \tag{S16}$$

Finally, elements of the solution vector $\boldsymbol{X}_B\left(\omega_b\right)$ are given by

$$Z_{bj} = \left[\frac{\partial\kappa_{bj}(\omega_b)}{\partial\varepsilon_B(\omega_b)}\right]_{\boldsymbol{\varepsilon}=\mathbf{0}} \;;\; Y_{bj}^* = \left[\frac{\partial\kappa_{bj}^*(-\omega_b)}{\partial\varepsilon_B(\omega_b)}\right]_{\boldsymbol{\varepsilon}=\mathbf{0}} \tag{S17}$$

The HF linear response function can now be built according to Eq. (S9).

## S1.4 Discussion

To extract excitation energies and transition moments from the approximate-state linear response function we introduce a non-singular matrix $X$ so that we may write[5,6]

$$\left[\frac{d^2Q}{d\varepsilon_A\left(-\omega\right)d\varepsilon_B\left(\omega\right)}\right]_{\boldsymbol{\varepsilon}=\mathbf{0}} = -\boldsymbol{E}_A^{[1]\dagger}X\left(X^\dagger E_0^{[2]}X - \hbar\omega X^\dagger S^{[2]}X\right)^{-1}X^\dagger\boldsymbol{E}_B^{[1]}.$$

The resolvent matrix can be brought to diagonal form upon solving the generalized eigenvalue problem

$$\left(E_0^{[2]} - \hbar\omega_m S^{[2]}\right)\boldsymbol{X}_m = 0, \tag{S18}$$

where $\mathbf{X}_m$ are columns of the matrix $X$, $\{\hbar\omega_m\}$ are interpreted as (approximate) excitation energies and

$$\boldsymbol{X}_m^\dagger\boldsymbol{E}_B^{[1]} \rightarrow \langle m|\hat{h}_B|0\rangle$$

corresponding transition moments. From the structure of the involved quantities, it is seen that eigensolutions come in pairs

$$\left\{ \omega_+ = +\left|\omega_m\right|, \boldsymbol{X}_{m,+} = \begin{bmatrix} Z \\ Y^* \end{bmatrix} \right\} \cup \left\{ \omega_- = -\left|\omega_m\right|, \boldsymbol{X}_{m,-} = \begin{bmatrix} Y \\ Z^* \end{bmatrix} \right\} \tag{S19}$$

In the general case one obtains

$$\boldsymbol{X}_{m,+}^\dagger \boldsymbol{E}_B^{[1]} = \boldsymbol{Z}^\dagger \boldsymbol{g}_B + \boldsymbol{Y}^T \boldsymbol{g}_B,$$

that is with both resonant and anti-resonant contributions. This is the case for HF response

$$\boldsymbol{X}_{m,+}^\dagger \boldsymbol{E}_B^{[1]} = -\sum_{ai} \left( \kappa_{ai}^{[1]*}\left(\omega_m\right) h_{B;ai} + \kappa_{ai}^{[1]}\left(-\omega_m\right) h_{B;ia} \right)$$

In the case of CI response, on the other hand, the off-diagonal blocks $B$ and $\Delta$ of the electronic Hessian $E_0^{[2]}$ and generalized metric $S^{[2]}$, respectively, are both zero, thus decoupling resonant and anti-resonant contribution, giving

$$\boldsymbol{X}_{m,+}^\dagger \boldsymbol{E}_B^{[1]} = -\sum_{n} S_{n0}^*\left(\omega_m\right) \langle n|\hat{h}_B|0\rangle.$$

In the exact case only $n = m$ contributes, with an arbitrary complex phase. In the HF-case $\Delta = 0$, whereas $B = 0$ is only achieved through the Tamm–Dancoff approximation.[7]

Further perspective on the form of transition moments in response theory is obtained by noting that the elements of the solution vectors are two-index quantities and can thereby be thought of as being selected from a matrix, hence inheriting the symmetries of that matrix. There is no particular symmetry, but we note that Hermitian and anti-Hermitian combinations can be formed from a solution vector $\boldsymbol{X}_{m,+}$ and its anti-resonant partner $\boldsymbol{X}_{m,-}$,

that is

$$\boldsymbol{X}_h = \frac{1}{2}\left(\boldsymbol{X}_{m,+} + \boldsymbol{X}_{m,-}\right) = \frac{1}{2}\begin{bmatrix} Z+Y \\ (Z+Y)^* \end{bmatrix}; \quad \boldsymbol{X}_a = \frac{1}{2}\left(\boldsymbol{X}_{m,+} - \boldsymbol{X}_{m,-}\right) = \frac{1}{2}\begin{bmatrix} Z-Y \\ -(Z-Y)^* \end{bmatrix},$$

which in turn means that a solution vector can be decomposed into Hermitian and anti-Hermitian parts. Since the elements of the property gradient, e.g. Eq. (S16), do come from a Hermitian matrix, we observe that its contraction with the Hermitian and anti-Hermitian parts of the solution vector gives transition moments that are real or imaginary, respectively

$$\boldsymbol{X}_h^\dagger \boldsymbol{E}_B^{[1]} = \mathrm{Re}\left[(\boldsymbol{Z}+\boldsymbol{Y})^\dagger \boldsymbol{g}_B\right]; \quad \boldsymbol{X}_a^\dagger \boldsymbol{E}_B^{[1]} = i\mathrm{Im}\left[(\boldsymbol{Z}-\boldsymbol{Y})^\dagger \boldsymbol{g}_B\right].$$

Interesting to note is that even though, as we have seen, the resonant and anti-resonant parts are strictly decoupled in the solution vectors of CI response theory, *this is not the case* when they are decomposed into Hermitian and anti-Hermitian parts.

Before closing it is worth mentioning that further insight and computational gains are obtained by decomposing the Hermitian and anti-Hermitian parts further into time reversal symmetric and anti-symmetic parts.[4,8] Letting $h = \pm 1$ indicate Hermiticity and $t = \pm 1$ indicate time reversal symmetry, one then observes

$$E_0^{[2]} \boldsymbol{X}(h,t) = \tilde{\boldsymbol{X}}(h,t); \quad S^{[2]} \boldsymbol{X}(h,t) = \tilde{\boldsymbol{X}}(-h,t).$$

Since the first-order response equation Eq. (S7) and the generalized eigenvalue problem Eq. (S18) are normally solved by expanding the solution vector in trial vectors, significant computational savings are obtained by restricting solution vectors to a particular time re-

versal symmetry $t$. With respect to transition moments, one furthermore finds that

$$\boldsymbol{X}^{\dagger}\left(h_1,t_1\right)\boldsymbol{E}_B\left(h_2,t_2\right)=\begin{cases}0 & h_1h_2=-t_1t_2\\ \text{real} & h_1h_2=t_1t_2=+1\\ \text{imaginary} & h_1h_2=t_1t_2=-1\end{cases}.$$

## S2 Conversion of Length and Velocity Representations

In this section, we will demonstrate that the *generalized* length and velocity representation can be interconverted according to Eq. (8) at the time-dependent Hartree–Fock (TD-HF) level of theory in the complete basis set limit, provided that the reference HF determinant is optimized, that is, Eq.(S13) is valid. This conversion has been carried out within the electric-dipole moment approximation in Ref. 9. Here, we will extend this derivation for electric-multipole moments to arbitrary order. We will use the second-quantization formalism, where, as above, $(i,j,k)$, $(a,b,c)$ and $(p,q,r,s)$ refer to occupied, virtual and general orbital indices.

Let us first consider how the two representations are related in exact-state theory. By invoking exact-state conditions, i.e., $\hat{H}|j\rangle = E_j|j\rangle$ we obtain

$$\langle f|\hat{\Omega}|i\rangle = \frac{1}{\hbar\omega_{fi}}\langle f|\left[\hat{H},\hat{\Omega}\right]|i\rangle = \langle f|\hat{\Gamma}|i\rangle. \tag{S20}$$

If we choose $\hat{\Omega} = \epsilon_p k_{j_1}\cdots k_{j_n}\hat{Q}^{[n+1]}_{j_1\cdots j_n;p}$, it follows that $\hat{\Gamma} = \epsilon_p k_{j_1}\cdots k_{j_n}\hat{\mathcal{Q}}^{[n+1]}_{j_1\cdots j_n;p}$, in line with Eq. (8). Therefore, the generalized length and velocity representation are equivalent for exact states.

For approximate methods, however, the second equality in Eq. (S20) does not always hold. In the basis set approximation, operators are represented as matrices and commutators of such matrices are only equal to the exact commutator in the complete basis set limit (more precise conditions are given in Ref. 10). Furthermore, approximate states are not eigenstates of the exact Hamiltonian, hence implying that Eq. (S20) does not apply in this situation.

This falsely suggests that in the complete basis set limit, transition moments in the length and velocity representation should not be equal in TD-HF theory. In practice, however, it has been observed that electric dipole transition moments in both representations become nearly equal for large basis sets.[11–15] We thus aim to demonstrate formally that at the TD-HF level these representations are strictly equivalent in the complete basis set limit.

A first guess would be to replace the Hamiltonian operator in Eq. (S20) with the Fock operator. In the canonical case, that is, $\hat{f}|\varphi_p\rangle = \varepsilon_p|\varphi_p\rangle$, we do find that

$$\langle\varphi_a|\left[\hat{f},\hat{\Omega}\right]|\varphi_i\rangle = (\varepsilon_a - \varepsilon_i)\langle\varphi_a|\hat{\Omega}|\varphi_i\rangle. \tag{S21}$$

However, if we select $-i\hbar\hat{\Omega} = \mathbf{r}$, the commutator $\left[\hat{f},\hat{\Omega}\right]$ not only gives the velocity operator, $\hat{\mathbf{p}}/m$ in the non-relativistic case, but also an exchange contribution, as observed already by Fock.[16] Notwithstanding, observing that the above difference of eigenvalues of the Fock operator appear in the diagonal blocks of the electronic Hessian in the canonical case

$$A_{ai,bj} = \delta_{ij}\delta_{ab}(\varepsilon_a - \varepsilon_i) - \mathcal{L}_{ab,ji}, \tag{S22}$$

the equivalence of the dipole length and dipole velocity representations in the complete basis limit can be shown for TD-HF;[17,18] for extensions to the Kohn–Sham and MCSCF case, the reader may consult Refs. 19 and 5, respectively. However, these proofs rely on the use of real orbitals, and the extension to the general length and velocity representations is not obvious.

We therefore follow a somewhat different path that will involve commutation with the total Hamiltonian (in second quantization) rather than the Fock operator. Let us first multiply Eq. (13) with the eigenvalue of the solution vector of the generalized eigenvalue problem, Eq.(S18) and insert the square of the generalized metric

$$\hbar\omega_{fi}\mathbf{X}^\dagger\mathbf{E}^{[1]}_\Omega = \hbar\omega_{fi}\mathbf{X}^\dagger S^{[2]}S^{[2]}\mathbf{E}^{[1]}_\Omega \tag{S23}$$

We can now substitute the generalized eigenvalue equation in this expression

$$\hbar\omega_{fi}\mathbf{X}^{\dagger}\mathbf{E}_{\Omega}^{[1]} = \begin{pmatrix} \boldsymbol{Z}^{\dagger} & \boldsymbol{Y}^{T} \end{pmatrix} \begin{pmatrix} A & B \\ B^{*} & A^{*} \end{pmatrix} \begin{pmatrix} \boldsymbol{g}_{\Omega} \\ -\boldsymbol{g}_{\Omega}^{*} \end{pmatrix}. \tag{S24}$$

After working out the matrix multiplications and grouping together the various commutators we obtain

$$\hbar\omega_{fi}\mathbf{X}^{\dagger}\mathbf{E}_{\Omega}^{[1]} = \sum_{ai} \left( Z_{ai}^{*} \langle \Phi_{i}^{a}| \left[\hat{H}, \hat{\Omega}^{\mathrm{ov}}\right] |\Phi_{0}\rangle + Y_{ai} \langle \Phi_{0}| \left[\hat{H}, \hat{\Omega}^{\mathrm{ov}}\right] |\Phi_{i}^{a}\rangle \right), \tag{S25}$$

where appears the reduced operator

$$\hat{\Omega}^{\mathrm{ov}} = \sum_{ai} \left( \Omega_{ai} \hat{a}_{a}^{\dagger} \hat{a}_{i} + \Omega_{ai}^{*} \hat{a}_{i}^{\dagger} \hat{a}_{a} \right) \tag{S26}$$

in which occupied-occupied (oo) and virtual-virtual (vv) blocks of $\Omega_{pq}$ are zero. In the following, it will be shown that in Eq. (S25) the reduced operator can be replaced with the full operator $\hat{\Omega}$. For these purposes, let us first consider the commutator of the Hamiltonian and the full operator and recognize that it has the same structure as Eq. (S10)

$$\left[\hat{H}, \hat{\Omega}\right] = \sum_{pq} h_{pq}^{\Omega} a_{p}^{\dagger} a_{q} + \sum_{pqrs} \frac{1}{4} \mathcal{L}_{pq,rs}^{\Omega} a_{p}^{\dagger} a_{r}^{\dagger} a_{s} a_{q}, \tag{S27}$$

where the integrals are now transformed with the elements of $\hat{\Omega}$ instead of $\hat{\kappa}$. To assess whether the full and reduced operator give the same result, we will proceed to compute the matrix elements from Eq. (S10) using the full operator. These matrix elements can be conveniently expressed in terms of the Fock matrix and the anti-symmetrized two-electron integrals

$$\langle \Phi_{i}^{a}| \left[\hat{H}, \hat{\Omega}\right] |\Phi_{0}\rangle = \sum_{t} \left[ \Omega_{at} F_{ti} - F_{at} \Omega_{ti} + \Omega_{jt} \mathcal{L}_{ai,tj} - \mathcal{L}_{ai,jt} \Omega_{tj} \right]. \tag{S28}$$

Here one should note that in the complete basis set limit resolution of the identity, $\sum_t |t\rangle\langle t| = 1$, gives equivalence with the commutator $\left[\hat{H}, \hat{\Omega}\right]$ in first quantization. Next, due to the variational condition, i.e. $F_{ia} = 0$, the terms depending on the oo and vv block of $\hat{\Omega}$ vanish

$$\langle \Phi_i^a | \left[\hat{H}, \hat{\Omega}\right] | \Phi_0 \rangle = \sum_j \Omega_{aj} F_{ji} - \sum_b F_{ab} \Omega_{bi} + \sum_{jb} \left[\Omega_{jb} \mathcal{L}_{ai,bj} - \mathcal{L}_{ai,jb} \Omega_{bj}\right]. \tag{S29}$$

The remaining terms thus depend only on the occupied-virtual/virtual-occupied blocks of $\hat{\Omega}$. We have thereby demonstrated the equivalence of matrix elements $\langle \Phi_i^a | \left[\hat{H}, \hat{\Omega}\right] | \Phi_0 \rangle$ and $\langle \Phi_i^a | \left[\hat{H}, \hat{\Omega}^{\text{ov}}\right] | \Phi_0 \rangle$. However, this is only valid if the summation in Eq. (S26) is complete over these blocks, which is notably *not* the case in the restricted excitation window approach employed in the present work.

In conclusion, we have made the following identification

$$\hbar\omega_{fi} \mathbf{X}^\dagger \mathbf{E}_\Omega^{[1]} = \mathbf{X}^\dagger \mathbf{E}_{[H,\Omega]}^{[1]} = \mathbf{X}^\dagger \mathbf{E}_\Gamma^{[1]}, \tag{S30}$$

where $\mathbf{E}_{[H,\Omega]}^{[1]}$ and $\mathbf{E}_\Gamma^{[1]}$ are the property gradients derived from the operators $[\hat{H}, \hat{\Omega}]$ and $\hat{\Gamma}$, respectively. Note that the second equality only holds in the complete basis set limit. If we choose $\hat{\Omega} = \epsilon_p k_{j_1} \cdots k_{j_n} \hat{Q}_{j_1 \cdots j_n ; p}^{[n+1]}$, this relation can then be used to convert the generalized length to the generalized velocity representation in the complete basis set limit. In Table I of the main text we do observe a significant difference between the oscillators strength of the generalized length and velocity representations. However, these results were obtained using a severely restricted excitation window as well as excitedd-state orbitals for which the variational condition $F_{ai} = 0$ does not hold. From Tables II and III we see that compliance with the variational condition is the most important factor in obtaining equivalence between the two representations.

## S3 Linear Dependences in Small Component Function

Throughout the main text, we advocate to use a tight linear dependence threshold for the calculations of radial distributions associated with truncated interaction. In this section, we will demonstrate what happens to the magnetic multipoles if the default linear dependence threshold in the DIRAC code is used ($10^{-6}$ for the large component space and $10^{-8}$ for the small component space).

Figure S1 shows the radial distributions of the magnetic multipole moments for the core transition. In these calculations, the default linear dependence threshold is applied, the effects of which are clearly visible: for $1 < n < 5$, the radial distributions of the dyall.ae3z and dyall.ae4z basis sets oscillate considerably around the numerical reference. At higher orders, the oscillations appear to less pronounced because the $r$-dependent prefactor dominates the characteristics of the curve. Although the oscillations are diminished in these curves, the overall deviations vastly increase. Interestingly, the basis set convergence seems to be inverted: larger basis sets introduce larger deviations from the numerical reference.

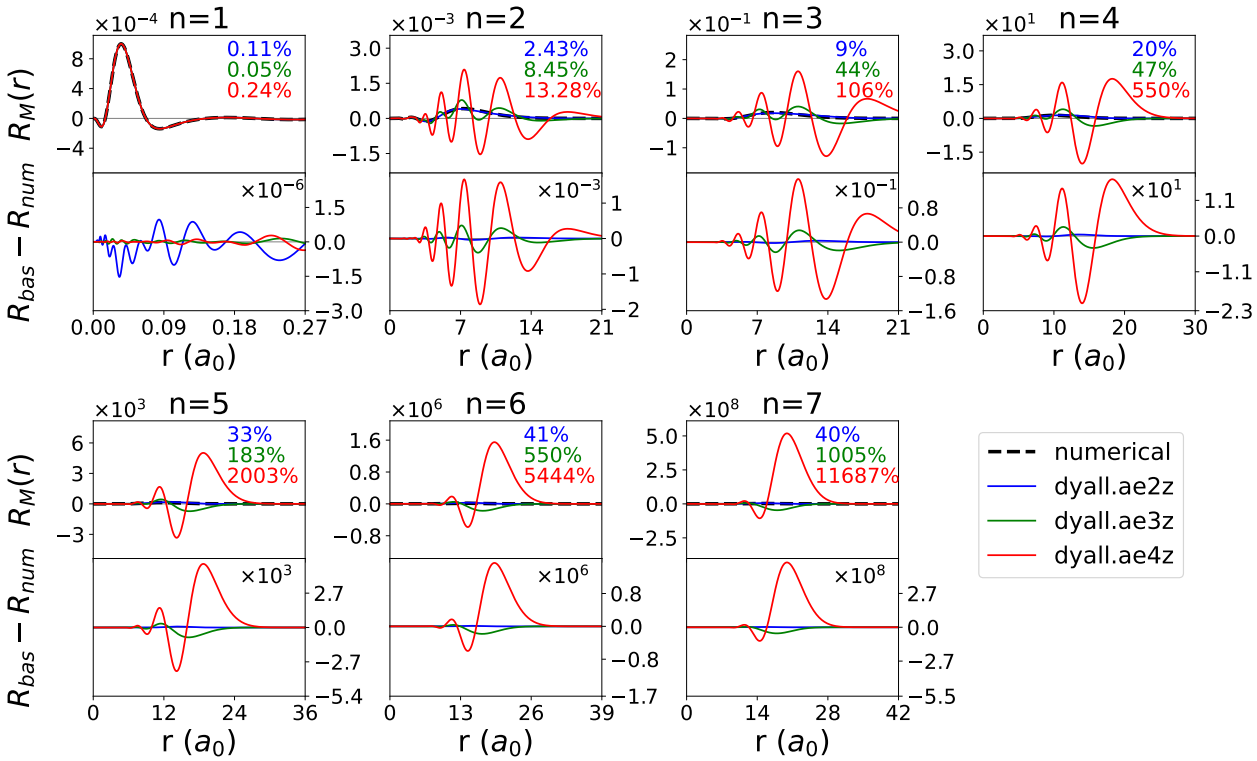


Figure S1: Core transition ($1s_{1/2} \rightarrow 7p_{1/2}$): radial distributions of magnetic multipole moments $\hat{m}^{[2n]}, n \in [1, 7]$. These distributions are calculated with the default linear dependence thresholds: $10^{-6}$ and $10^{-8}$ for the large and small component space. In each box, the upper panel contains the radial distribution, while the lower panel contains error relative to the numerical reference. Note that each box has different scales. The percentages in the upper right corner of each box are the relative errors of the transition moments, i.e. $|\frac{T_{\text{bas}} - T_{\text{num}}}{T_{\text{num}}}| \times 100\%$.

To understand the origin of these oscillations, we need to analyze the orbitals involved (Figure S2). The $7p_{1/2}$ orbital converges smoothly towards the numerical reference, whereas the error curve of the $1s_{1/2}$ orbital exhibit similar oscillations as the magnetic multipoles. Especially the basis set convergence of the small component of the $1s_{1/2}$ orbital is problematic: instead of reducing the error, the dyall.ae3z and dyall.ae4z deteriorate the description of the small component function. It seems that most of the oscillations in Figure S1 stem from the small component of the $1s_{1/2}$ orbital. Therefore, in the following, we inspect the $Q_{1,-1}$ function in terms of its basis set expansion.

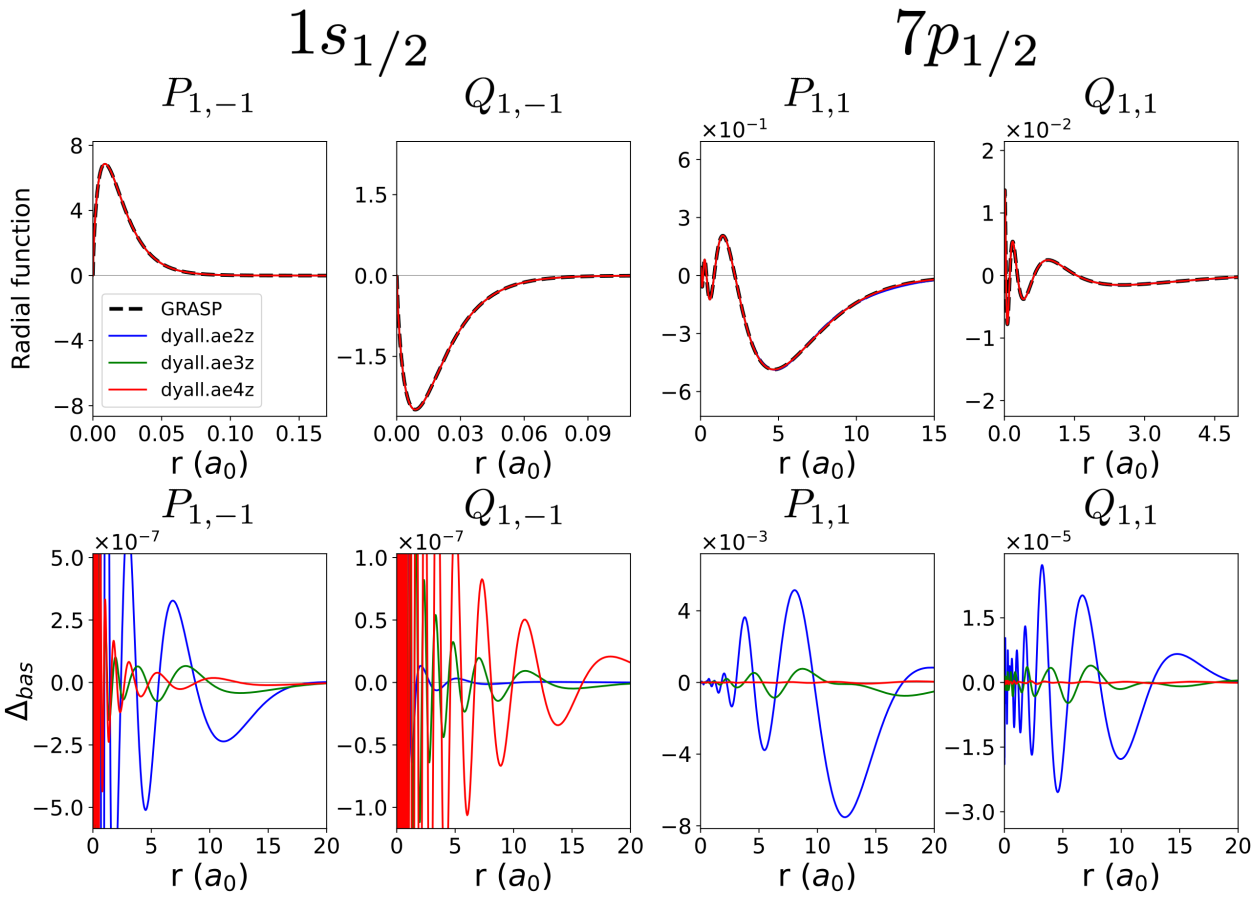


Figure S2: Radial functions of the large and small component of the $1s_{1/2}$ ($\langle r \rangle = 0.01454\ a_0$)and $7p_{1/2}$ orbital (top row) and their deviations from the numerical reference (bottom row). These orbitals were taken from the radium atom with [Ra]$1s^{-1}_{1/2}7p^{1}_{1/2}$ configuration. The basis set orbitals were calculated at the 4c-HF level using DIRAC, while the numerical reference was calculated with GRASP. These calculations where carried out using the default linear dependence threshold: $10^{-6}$ and $10^{-8}$ for the large and small component space. Note that the scaling is different for each individual box and that the error curves are plotted in a different range than the radial functions.

Ideally, we want to expand the large and small component in a two-component basis

$$\mathcal{G}_{\alpha\kappa\ell m} = R_{\alpha\ell}(r)\xi_{\kappa m}(\theta,\phi), \tag{S31}$$

where the radial part is a Gaussian function

$$R_{\alpha\ell} = N_{\alpha\ell} r^{\ell} e^{-\alpha r^2}; \quad N_{\alpha l} = \frac{2(2\alpha)^{3/4}}{\pi^{1/4}} \sqrt{\frac{2^{\ell}}{(2\ell+1)!!}} \left(\sqrt{2\alpha}\right)^{\ell} \tag{S32}$$

and the angular part a spherical spinor, depending on the angular quantum numbers $\kappa$ and $m$. However, in its current form, Eq. (S31) cannot be used as a basis for the small component function, because the condition of restricted kinetic balance is not fulfilled. It is well-known that violation of this principle can lead to variational collapse.[20,21] A proper radial basis for the small component function reads[22]

$$R^S \propto \begin{cases} \sqrt{2\ell+3}R_{\alpha,\ell^L+1} - 2\sqrt{2\ell+1}R_{\alpha,\ell^L-1} & \text{for } \kappa^L = \ell^L > 0 \\ R_{\alpha,\ell^L+1} & \text{for } \kappa^L = -(\ell^L+1) < 0, \end{cases} \tag{S33}$$

As an example, for small component $\ell^S = 1$, the latter function, generated from $\ell^L = 0$, is to be used for $p_{1/2}$ and the former, generated from $\ell^L = 2$, for $p_{3/2}$. In the atomic case, the 2-component basis functions do not mix since they have different angular parts, corresponding to $\kappa^S = +1$ and $\kappa^S = -2$, respectively.

However, in the DIRAC code, a scalar basis is employed

$$G_{\alpha\ell m} = R_{\alpha\ell}(r)Y_{\ell m}(\theta,\phi), \tag{S34}$$

Small component basis functions with radial parts corresponding to both forms of Eq. (S33) are generated, hence adhering to kinetic balance. However, now, in the case of e.g. $\ell^S = 1$, basis functions can contribute to both $p_{1/2}$ and $p_{3/2}$, hence possibly amplifying linear dependencies.

# S4 Augmented Basis Sets

In the main text, we have investigated the absolute basis set convergence of the full interaction operator and the various multipole moments. In general, we have observed that the high-order multipole moments require at least the dyall.ae4z basis set. However, compared to the dyall.ae2z basis set, the dyall.ae4z basis contains additional tight functions, in addition

to functions of higher orbital angular momentum, that may not contribute to the high-order multipole moments. Therefore, we investigated the effects of augmenting the dyall.ae2z basis set, such that a better balance could be found between accuracy and basis set size. We have employed two schemes to construct a new basis set:

I Adding diffuse functions to the dyall.ae2z basis set in an even-tempered fashion.

II Replacing the diffuse functions of the dyall.ae2z basis set with the diffuse functions of the larger basis sets. This scheme is inspired by recent work of Jensen and coworkers[23] in which they augmented the cc-pVnZ basis set with the core polarization functions of the cc-pCV(n+1)Z basis set.

In Table S1, the exponents and the shell of the augmentation functions from Scheme I are depicted. Because the dyall.aeXz basis sets are constructed from uncontracted functions, there is no need to give contraction coefficients in Table S1. To generate the augmentation functions, we took the ratio of the two most diffuse exponents. The exponents of the augmentation functions are obtained by multiplying an integer multiple of this ratio with the most diffuse exponent. Table S2 summarizes the composition of the basis sets from Scheme II. These basis sets are constructed by replacing the $N$ most diffuse functions from the dyall.ae2z basis set with the $M$ most diffuse functions of the dyall.ae3z or dyall.ae4z basis set. Accordingly, these basis sets are named ae2z+dae3z and ae2z+dae4z, respectively. In the construction of these bases, $M$ is always chosen larger than $N$, hence creating a larger basis set than the original. However, there remains a certain degree of arbitrariness in the construction of the basis sets in Scheme II, because there is not a general method to decide how many functions to remove and introduce. Jensen and coworkers did not face this problem, because the cc-pcVnZ basis sets are constructed by introducing core-polarization functions to the cc-pVnZ basis set. Therefore, the augmentation of the cc-pVnZ basis set with the core polarization functions of the cc-pCV(n+1)Z basis set is not ambiguous.

Table S1: Exponents of the augmentation functions used for the basis sets of Scheme I. The letters $s$ and $p$ denote the shell of the augmentation functions. Numbers in parentheses are exponents of 10.

| | $s_1$ | $s_2$ | $s_3$ | $p_1$ | $p_2$ | $p_3$ |
|---|---|---|---|---|---|---|
| Exponent | 8.672(−3) | 3.669(−3) | 1.552(−3) | 7.304(−3) | 2.821(−3) | 1.089(−3) |

Table S2: Composition of the hybrid basis sets from Scheme II. The third column summarizes how many diffuse functions from the dyall.ae2z were removed ($N$), while the fourth column indicates the number of diffuse functions that were added ($M$) from the dyall.aeXz ($X = 3, 4$) basis set.

| Basis | shell | $N$ | $M$ |
|---|---|---|---|
| ae2z+dae3z | $s$ | 9 | 11 |
| | $p$ | 8 | 10 |
| ae2z+dae4z | $s$ | 8 | 12 |
| | $p$ | 8 | 12 |

To assess the performance of these composite basis sets, we computed the radial distributions of the length representation electric and magnetic transition multipole moments for the $1s_{1/2} \rightarrow 7p_{1/2}$ transition. The results of Scheme I are depicted in Figures S3 and S4, respectively. In both figures, the augmented basis sets have similar performance for the first two orders. For $n = 2$ and $n = 3$, the augmented basis sets seem to induce small oscillations with respect to the numerical reference. At the three highest orders, the augmented basis sets completely fail to capture the shape of the reference due to severe oscillations, despite the use of tight thresholds for linear dependence. Thus, we conclude that the basis sets from Scheme I are not a proper substitute for the dyall.ae3z and dyall.ae4z basis sets.

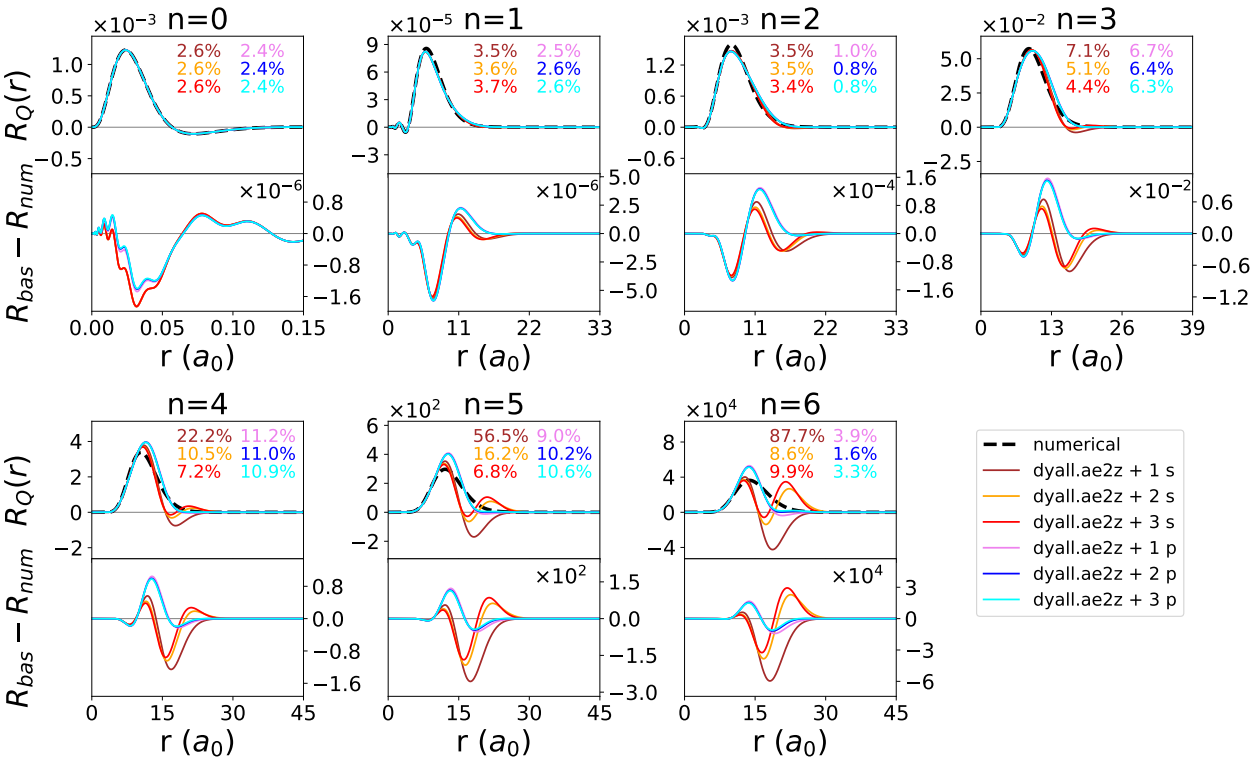


Figure S3: Scheme I. Radial distributions of electric transition multipole moments in the generalized length representation for the $1s_{1/2} \rightarrow 7p_{1/2}$ transition. The basis sets for these calculations were generated by augmenting the dyall.ae2z basis set with diffuse functions in an even-tempered fashion. The percentages in the upper right corner of each box are the relative errors of the transition moments, i.e. $|\frac{T_{\mathrm{bas}} - T_{\mathrm{num}}}{T_{\mathrm{num}}}| \times 100\%$.

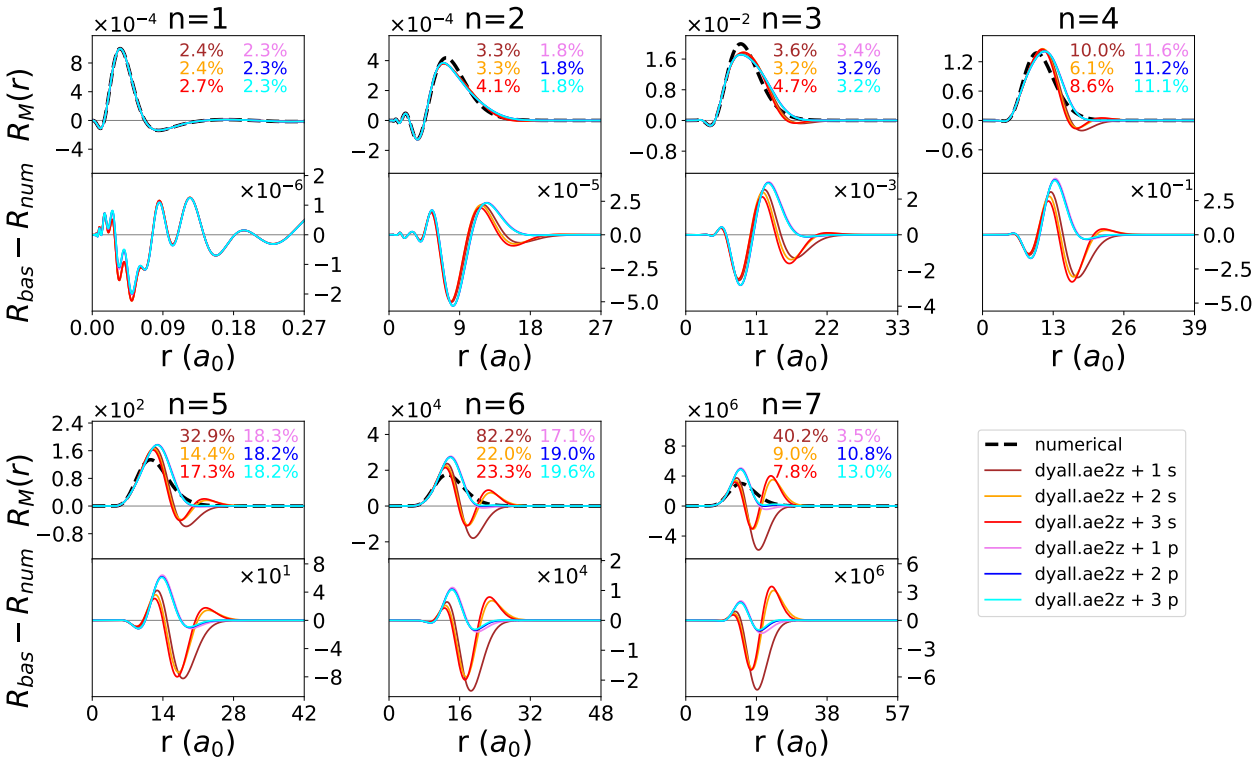


Figure S4: Scheme I. Radial distributions of magnetic transition multipole moments for the $1s_{1/2} \rightarrow 7p_{1/2}$ transition. The basis sets were generated by augmenting the dyall.ae2z basis set with diffuse functions in an even-tempered fashion. The percentages in the upper right corner of each box are the relative errors of the transition moments, i.e. $|\frac{T_{\rm bas}-T_{\rm num}}{T_{\rm num}}|\times 100\%$.

Figures S5 and S6 depict the results from Scheme II for the length representation electric and magnetic transition multipole moments, respectively. The basis sets constructed with this scheme provide no obvious improvement over the dyall.ae2z basis sets. Therefore, Scheme II is not a suitable alternative to the dyall.ae3z and dyall.ae4z basis sets.

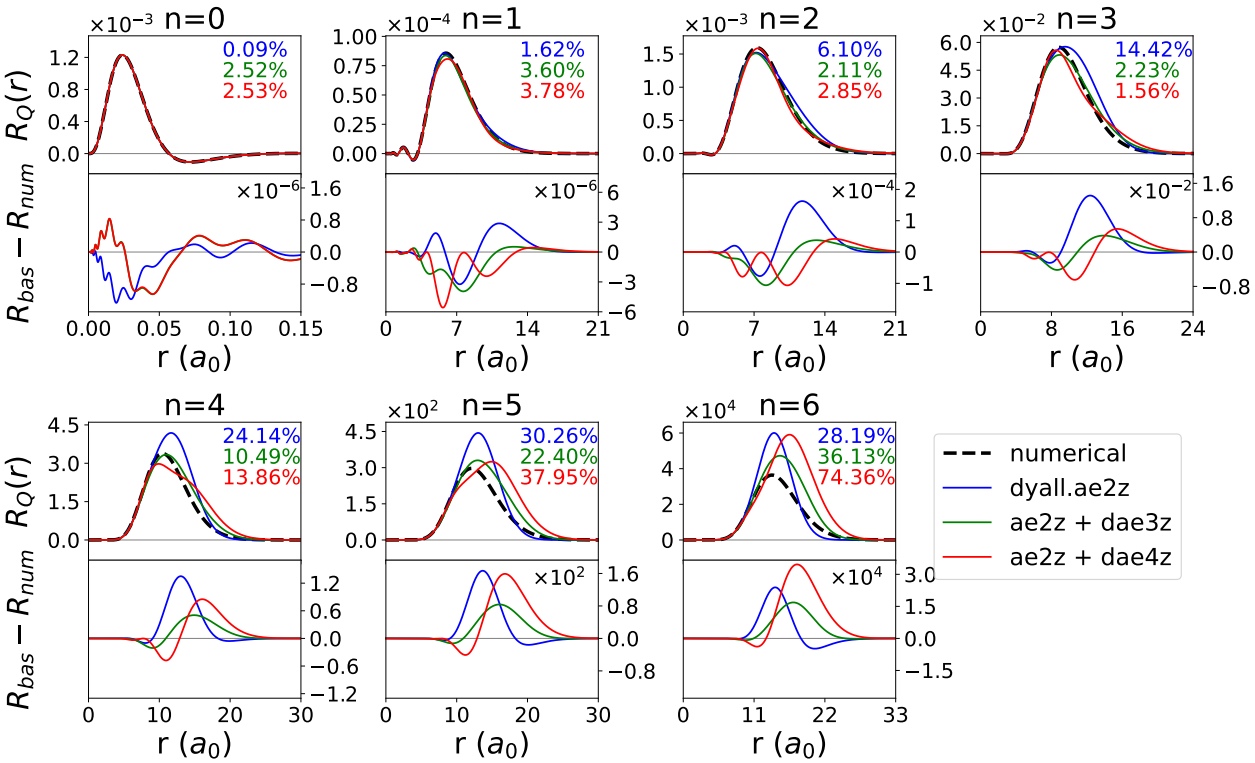


Figure S5: Scheme II. Radial distributions of electric transition multipole moments in the generalized length representation for the $1s_{1/2} \rightarrow 7p_{1/2}$ transition. The basis sets for these calculations were generated by augmenting the dyall.ae2z basis set with the diffuse functions of either the dyall.ae3z or dyall.ae4z basis sets. The percentages in the upper right corner of each box are the relative errors of the transition moments, i.e. $|\frac{T_{\rm bas}-T_{\rm num}}{T_{\rm num}}|\times 100\%$.

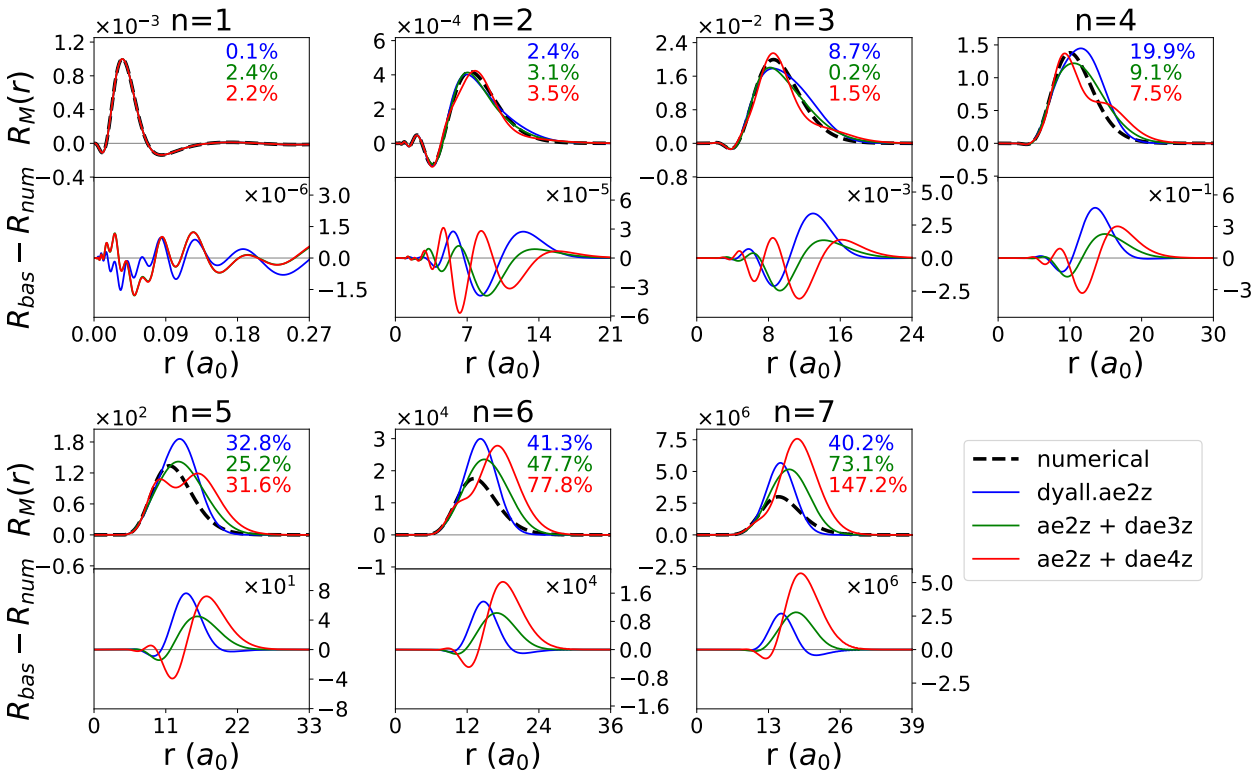


Figure S6: Scheme II. Radial distributions of magnetic transition multipole moments for the $1s_{1/2} \rightarrow 7p_{1/2}$ transition. The basis sets for these calculations were generated by augmenting the dyall.ae2z basis set with the diffuse functions of either the dyall.ae3z or dyall.ae4z basis sets. The percentages in the upper right corner of each box are the relative errors of the transition moments, i.e. $|\frac{T_{\text{bas}} - T_{\text{num}}}{T_{\text{num}}}| \times 100\%$.

# References


(1) Patrick Norman and Kenneth Ruud and Trond Saue, *Principles and Practices of Molecular Properties: Theory, Modeling and Simulations*; Wiley: Hoboken, NJ, 2018; DOI: doi:10.1002/9781118794821.

(2) Langhoff, P. W.; Epstein, S. T.; Karplus, M. Aspects of Time-Dependent Perturbation Theory. *Rev. Mod. Phys.* **1972**, *44*, 602–644, DOI: doi:10.1103/RevModPhys.44.602.

(3) Christiansen, O.; Jørgensen, P.; Hättig, C. Response Functions from Fourier Component Variational Perturbation Theory Applied to a Time-Averaged Quasienergy. *Int. J.*

*Quant. Chem.* **1998**, *68*, 1–52, DOI: doi:10.1002/(SICI)1097-461X(1998)68:1<1::AID-QUA1>3.0.CO;2-Z.

(4) Saue, T. In *Relativistic Electronic Structure Theory. Part 1. Fundamentals*; Schwerdtfeger, P., Ed.; Elsevier: Amsterdam, 2002; p 332, DOI: doi:10.1016/S1380-7323(02)80033-4.

(5) Olsen, J.; Jørgensen, P. Linear and nonlinear response functions for an exact state and for an MCSCF state. *The Journal of chemical physics* **1985**, *82*, 3235–3264, DOI: doi:10.1063/1.448223.

(6) Bast, R.; Jensen, H. J. Aa.; Saue, T. Relativistic adiabatic time-dependent density functional theory using hybrid functionals and noncollinear spin magnetization. *International Journal of Quantum Chemistry* **2009**, *109*, 2091–2112, DOI: doi:10.1002/qua.22065.

(7) Dunning, T. H.; McKoy, V. Nonempirical Calculations on Excited States: The Ethylene Molecule. *J. Chem. Phys.* **1967**, *47*, 1735, DOI: doi:10.1063/1.1712158.

(8) Saue, T.; Jensen, H. J. Aa. Linear response at the 4-component relativistic level: Application to the frequency-dependent dipole polarizabilities of the coinage metal dimers. *The Journal of Chemical Physics* **2003**, *118*, 522–536, DOI: doi:10.1063/1.1522407.

(9) Linderberg, J.; Öhrn, Y. *Propagators in quantum chemistry*, 2nd ed.; John Wiley & Sons, 2004; pp 86–88, DOI: doi:10.1002/0471721549.

(10) Dyall, K. G.; Grant, I. P.; Wilson, S. Matrix representation of operator products. *J. Phys. B* **1984**, *17*, 493, DOI: doi:10.1088/0022-3700/17/4/006.

(11) Sørensen, L. K.; Guo, M.; Lindh, R.; Lundberg, M. Applications to metal K pre-edges of transition metal dimers illustrate the approximate origin independence for the

intensities in the length representation. *Molecular Physics* **2017**, *115*, 174–189, DOI: doi:10.1080/00268976.2016.1225993.

(12) Sørensen, L. K.; Guo, M.; Lindh, R.; Lundberg, M. Applications to metal K pre-edges of transition metal dimers illustrate the approximate origin independence for the intensities in the length representation. *Molecular Physics* **2017**, *115*, 174–189, DOI: doi:10.1080/00268976.2016.1225993.

(13) Sørensen, L. K.; Lindh, R.; Lundberg, M. Gauge origin independence in finite basis sets and perturbation theory. *Chemical Physics Letters* **2017**, *683*, 536–542, DOI: doi:10.1016/j.cplett.2017.05.003.

(14) Sørensen, L. K.; Kieri, E.; Srivastav, S.; Lundberg, M.; Lindh, R. Implementation of a semiclassical light-matter interaction using the Gauss-Hermite quadrature: A simple alternative to the multipole expansion. *Physical Review A* **2019**, *99*, 013419, DOI: doi:10.1103/PhysRevA.99.013419.

(15) List, N. H.; Melin, T. R. L.; van Horn, M.; Saue, T. Beyond the electric-dipole approximation in simulations of x-ray absorption spectroscopy: Lessons from relativistic theory. *The Journal of chemical physics* **2020**, *152*, 184110, DOI: doi:10.1063/5.0003103.

(16) Fock, V. Über die Anwendbarkeit des quantenmechanischen Summensatzes. *Zeitschrift für Physik* **1934**, *89*, 744–749, DOI: doi:10.1007/BF01341387.

(17) Harris, R. A. Oscillator Strengths and Rotational Strengths in Hartree–Fock Theory. *The Journal of Chemical Physics* **1969**, *50*, 3947–3951, DOI: doi:10.1063/1.1671653.

(18) Starace, A. F. Length and Velocity Formulas in Approximate Oscillator-Strength Calculations. *Phys. Rev. A* **1971**, *3*, 1242–1245, DOI: doi:10.1103/PhysRevA.3.1242.

(19) Furche, F. On the density matrix based approach to time-dependent density func-

tional response theory. *The Journal of Chemical Physics* **2001**, *114*, 5982–5992, DOI: doi:10.1063/1.1353585.

(20) Asaad, W. Relativistic K Electron Wave Functions by the Variational Principle. *Proceedings of the Physical Society (1958-1967)* **1960**, *76*, 641, DOI: doi:10.1088/0370-1328/76/5/304.

(21) Kim, Y.-K. Relativistic self-consistent-field theory for closed-shell atoms. *Physical Review* **1967**, *154*, 17, DOI: doi:10.1103/PhysRev.154.17.

(22) Dyall, K. G.; Fægri Jr, K. *Introduction to relativistic quantum chemistry*; Oxford University Press, 2007; pp 198–204, DOI: doi:10.1093/oso/9780195140866.001.0001.

(23) Ambroise, M. A.; Dreuw, A.; Jensen, F. Probing basis set requirements for calculating core ionization and core excitation spectra using correlated wave function methods. *Journal of Chemical Theory and Computation* **2021**, *17*, 2832–2842, DOI: doi:10.1021/acs.jctc.1c00042.